Journal Name

ARTICLE TYPE

Cite this: DOI: 10.1039/xxxxxxxxxx

Chemical Bonding in Cuprous Complexes with Simple Nitriles: Octet Rule and Resonance Concepts versus Quantitative Charge-Redistribution Analysis

Simone Potenti[a], Lorenzo Paoloni[a], Surajit Nandi[a], Marco Fusè [a], Vincenzo Barone[ab], and Sergio Rampino*[ab]

Received Date
Accepted Date

DOI: 10.1039/xxxxxxxxxx

www.rsc.org/journalname

Chemical bonding in a set of six cuprous complexes with simple nitriles (CN^-, HNC, HCN, CH_3NC, and CH_3CN) is investigated by means of a recently devised analysis scheme framed in density-functional theory and quantitatively singling out concurrent charge flows such as σ donation and π backdonation. The results of our analysis are comparatively assessed against qualitative models for charge redistribution based on the popular concepts of octet rule and resonance structures, and the relative importance of different charge-flow channels relating to σ donation, π back-donation, polarization, and hyperconjugation is discussed on a quantitative basis.

1 Introduction

The reconciliation between intuitive chemical concepts, such as resonance or back-donation, and the results of quantum mechanical computations is still one central issue in the interpretation of a wealth of chemical phenomena where chemical bonding plays a central role. As a matter of fact, one of the first successful attempts in describing chemical bonds dates back to 1916, when Gilbert N. Lewis developed the concept of electron-pair bond[1,2]. When applied to light elements, this approach leads to compounds usually featuring eight valence (outer-shell) electrons around each atom, according to a trend which was first noticed in 1904 by Richard Abegg[3]. After Lewis' paper in 1916, this common behavior underwent further investigation, and in 1919 Irving Langmuir refined it introducing the concepts of "cubical octet atom" and "octet theory"[4], the latter evolving into what is now known as the "octet rule". As widely recognized, the octet rule, together with the valence-shell electron-pair repulsion (VSEPR) theory[5,6], proved to be very robust especially in the field of molecular-geometry investigation, but it kept on failing in properly describing some systems, such as benzene, until the concept of resonance was introduced into quantum mechanics by Werner Heisenberg in 1926[7] and then used in 1928 by Linus Pauling to explain the partial valence of molecules[8–10]. Later on, other empirical rules were introduced dealing with 12-22 electrons for a better description of chemical bonds involving transition metals, with the 18-electron rule first proposed by Langmuir in 1921[11] being the most popular.

With the advent of quantum mechanics and, more recently, the revolution in scientific computing and visualization brought by modern technology, increasingly refined approaches based on the physics of atoms and molecules have been developed for a quantum-mechanical description of chemical bonding. Some of these methods (for a general discussion see Ref. 12) focus on energy partitioning (SAPT[13,14], EDA[15]), some others on the topology of the electron density (QTAIM[16]), some others on the wavefunction (ELF[17], ELI-D[18]). We have recently focussed our attention on a novel promising analysis scheme combining an orbital-space and a real-space analysis of the electron-charge redistribution upon intermolecular interactions. We have also integrated it with state-of-the-art virtual-reality technology, thus realising the first virtual laboratory for the immersive analysis of chemical bonding[19,20]. The above mentioned technique has been successfully used in several studies especially in the field of coordination chemistry, where it provided a robust quantitative framework for singling out competitive charge flows as the σ donation and π back-donation[21–24] (see also Refs. 25–27 for application in other contexts). Similar methods – targeting chemical bonding from the perspective of the rearrangement of the electrons –

[a] *Scuola Normale Superiore, SMART Laboratory, Piazza dei Cavalieri 7, 56126 Pisa, Italia. Tel: +39 050 509 071; E-mail: sergio.rampino@sns.it*
[b] *Istituto Nazionale di Fisica Nucleare (INFN) – Sezione di Pisa, Largo Bruno Pontecorvo 3, 56127 Pisa, Italia.*

represent the quantum-mechanical counterpart of the previously-mentioned widely adopted qualitative models, and offer nowadays the unprecedented possibility of a one to one comparison with these latter and a great chance for a deep insight in the nature of the studied chemical bonds.

In this work, we set out to contribute to the bridging of chemical concepts and quantum mechanics by investigating chemical bonding in cuprous complexes with simple nitriles and comparing the results of a qualitative model based on the octet rule and resonance concepts with those of the above-mentioned quantitative scheme based on quantum-mechanical calculations within a density-functional theory (DFT) framework. To this purpose, we consider a set of complexes where the cuprous ion Cu^+ binds the following simple C_1 and C_2 nitriles:

- cyanide anion (bound to Cu^+ via both C and N, leading to cuprous cyanide and isocyanide, species **1** and **2** of Table 1),
- hydrogen cyanide HCN and isocyanide HNC (leading to species **3** and **4**),
- acetonitrile CH_3CN and methyl isocyanide CH_3NC (leading to species **5** and **6**).

Table 1: Summary of the analyzed species, ligands, and bonds

Species	Ligand	Studied bond
1 $Cu-C\equiv N$	Cyanide anion CN^-	$Cu-C$
2 $Cu-\overset{\oplus}{N}\equiv\overset{\ominus}{C}$		$Cu-N$
3 $Cu-C\equiv\overset{\oplus}{N}-H$	Hydrogen isocyanide HNC	$Cu-C$
4 $Cu-\overset{\oplus}{N}\equiv C-H$	Hydrogen cyanide HCN	$Cu-N$
5 $Cu-C\equiv\overset{\oplus}{N}-CH_3$	Methyl isocyanide CH_3NC	$Cu-C$
6 $Cu-\overset{\oplus}{N}\equiv C-CH_3$	Acetonitrile CH_3CN	$Cu-N$

The set of complexes has been conceived by adding complexity to the simple copper(I) cyanide, which is an important reagent in organic, organometallic, and supramolecular chemistry[28], through a series of ligands that have relevance on their own: the highly toxic cyanide anion[29] is a common ligand for many transition metals[30]; both hydrogen cyanide and isocyanide attract growing interest in the field of astrochemistry[31–33], mainly as far as the HCN/HNC ratio and isomerization are concerned[34–37]; acetonitrile is commonly used as a polar aprotic solvent or as two-carbon building block in organic synthesis[38], and it is an easily displaceable ligand commonly used in catalysis[39]. As detailed later on in the article, this last ligand together with methyl isocyanide were chosen so as to probe the hyperconjugation phenomenon[40].

The article is organized as follows. In Section 2, the bond-analysis technique is briefly reviewed and computational details are given. In Section 3, the resonance structures for the considered complexes are discussed. In Section 4, the resonance structures are comparatively assessed against the results of quantitative charge-redistribution analysis. Conclusions are drawn in Section 5.

2 Methodology

2.1 Orbital-space/real-space bond analysis

The bond-analysis technique adopted in this work has been firstly presented in Ref. 41, and has been recently extended to the fully relativistic theoretical framework[42] for use in four-component relativistic DFT calculations[43,44]. For the reader's convenience, the method is briefly outlined in the following.

In our scheme, the charge redistribution upon bonding of two fragments A and B is formulated as the difference $\Delta\rho(x,y,z)$ between the electron density of the adduct AB and a reference density associated with the non-interacting fragments taken at their in-adduct geometries. Such reference density is constructed from occupied molecular orbitals of the non-interacting fragments made orthonormal to each other. If all densities are computed from single-determinant wavefunctions (as in Hartree-Fock or DFT calculations), $\Delta\rho$ can be decomposed into weighed contributions coupling pairs of new molecular orbitals $\varphi_{\pm k}(x,y,z)$ (so-called natural orbitals for chemical valence, NOCVs[45,46]):

$$\Delta\rho = \sum_k w_k \left(|\varphi_k|^2 - |\varphi_{-k}|^2 \right) = \sum_k w_k \Delta\rho_k \,, \qquad (1)$$

where we dropped the spatial dependence of densities and orbitals for clarity. In other words, the total electron charge rearrangement $\Delta\rho$ taking place upon the fragment-fragment interaction is decomposed into additive charge flows of w_k electrons flowing from orbital φ_{-k} to orbital φ_k, with k ranging from one to the number of occupied molecular orbitals of the adduct. Only a few NOCV components in Eq. 1 have a significant weight and thus contribute non-negligibly to the overall charge rearrangement. The chemical character of these contributions can be recognized by a visual inspection in 3D space of the related electron-density differences.

While the above-sketched analysis provides an informative qualitative picture of the several components making up the overall charge redistribution, each of these 'charge-flow channels' can then be quantitatively analyzed in real-space by computing the associated charge-flow profile along a given axis z (commonly chosen as the interaction axis) through the following progressive partial integration:

$$\Delta q_k(z) = w_k \int_{-\infty}^{z} \mathrm{d}z' \int_{-\infty}^{\infty}\int_{-\infty}^{\infty} \Delta\rho_k(x,y,z')\ \mathrm{d}x\ \mathrm{d}y \,. \qquad (2)$$

For each z point along the axis, the resulting function $\Delta q_k(z)$ is by definition the exact amount of electron charge that has crossed from right to left a plane orthogonal to the z axis through that point.[47,48]. It is often useful to define a boundary between fragments A and B in order to get clear-cut estimates of the inter-fragment charge transfer (CT) associated with each charge-flow component: such boundary is commonly defined as the z point where equal-valued isodensity surfaces of the isolated A and B fragments become tangent (the resulting CT is then the value of $\Delta q_k(z)$ at that z point).

Table 2: Optimized bond lengths (in Å) and harmonic frequencies (ω in cm^{-1}) of the six considered compounds. The weights of the main resonance structures according to the natural resonance theory are reported in brackets.

Species		Bond length		ω
		B3	DH	DH
1 Cu — C ≡ N (90.9 %)	$r_{C\equiv N}$	1.1685	1.1677	2174.18
	r_{Cu-C}	1.8550	1.8178	482.18
2 Cu — $\overset{\oplus}{N}$ ≡ $\overset{\ominus}{C}$ (95.4 %)	$r_{C\equiv N}$	1.1837	1.1796	2105.08
	r_{Cu-N}	1.8231	1.7798	509.77
3 Cu — C ≡ $\overset{\oplus}{N}$ — H (95.4 %)	$r_{C\equiv N}$	1.1562	1.1530	2209.69
	r_{N-H}	1.0101	1.0069	
	r_{Cu-C}	1.9050	1.8553	409.77
4 Cu — $\overset{\oplus}{N}$ ≡ C — H (96.1 %)	$r_{C\equiv N}$	1.1520	1.1491	2194.25
	r_{C-H}	1.0781	1.0747	
	r_{Cu-N}	1.9041	1.8542	397.57
5 Cu — C ≡ $\overset{\oplus}{N}$ — CH_3 (79.0 %)	$r_{C\equiv N}$	1.1574	1.1552	2319.15
	r_{N-C}	1.4302	1.4351	
	r_{C-H}	1.0928	1.0879	
	r_{Cu-C}	1.8947	1.8502	351.90
6 Cu — $\overset{\oplus}{N}$ ≡ C — CH_3 (82.3 %)	$r_{C\equiv N}$	1.1581	1.1540	2346.04
	r_{C-C}	1.4524	1.4528	
	r_{C-H}	1.0954	1.0905	
	r_{Cu-N}	1.8882	1.8416	347.11

2.2 Computational details

Most of the calculations reported in this article were performed using density-functional theory (DFT) with the Gaussian suite of programs (G16 Rev. C.01)[49], adopting the B3LYP[50,51] exchange-correlation functional and accounting for dispersion contributions by means of the Grimme's D3BJ[52] model as implemented in Gaussian. Calculations were performed in vacuo using a LANL2DZ basis set with effective core potential for Cu[53] and a 6-31+G* basis set for H, C, and N[54,55] (hereafter B3). Although more advanced methods (e.g. double hybrid functionals[56] or post-Hartree-Fock composite methods[57,58] could provide more accurate quantitative results, general trends (which are the main topic of the present study) should be well reproduced by the chosen computational level. This statement is confirmed by the results collected in Tab. 2, where geometrical parameters computed at the B3 level are compared with their counterparts issuing from rev-DSD-PBEP86 double hybrid[59] computations in conjunction with the jun-cc-pVTZ basis set[60] for H, C, N and the aug-pp-cVTZ basis set[61] with the SDD pseudopotential[62] on Cu (hereafter DH). The same Table collects also DH harmonic frequencies (which are often used to estimate bond strengths) and the weigths of the main resonances structures (labelled with letter **a** in the following) obtained by the natural resonance theory (NRT)[63]. NRT and natural energy decomposition analysis (NEDA)[64–66] were performed with NBO 7.0 program[67] interfaced with the Gaussian suite of programs.

Very few experimental results are available for this class of compounds, the only notable exception being CuCN. In this case a very accurate semi-experimental structure is available[28,68], whose geometrical parameters (CuC=1.8287 and CN=1.1636 Å) are in fair agreement with B3 values and in good agreement with DH ones. Also the experimental harmonic frequencies[28] (2192.4 and 478 cm^{-1} for the CN and CuC stretching, respectively) are in good agreement with DH values.

After reorienting the optimized structure of each complex so as to have Cu on the origin of the reference frame and all other atoms on the positive z semi-axis, single-point calculations were run both for the adduct and its two constituting fragments (i.e., Cu^+ and the related ligand of Table 1) frozen at their in-adduct geometry (i.e., already deformed from their respective equilibrium structure; see also the activation strain/distortion-interaction model on this[69]), in order to compute the respective electron densities. Note that in defining the fragments we opted for heterolytic (rather than homolytic) bond cleavage because, as shown in Ref. 70 and confirmed by our NRT calculations, the bonding situation in the considered complexes is better described using charged (rather than neutral) fragments.

NOCVs were then computed through a parallel version of program Waverley[71] and subsequently analyzed through immersive sessions in our virtual laboratory. Numerical integration (Eq. 2) was performed by discretizing the integrand onto a 3D-grid with sampling intervals 0.2, 0.2, and 0.1 Bohr for x, y, and z, respectively, in a suitably-chosen region of space (a box encompassing the whole structure with an additional margin of 6.0 Bohr on each side) using a finite scheme through the procedures of the CUBES library and program suite[72] as integrated in our virtual laboratory[19].

3 Resonance structures

Judging the relative significance (i.e. contribution to resonance hybrid) of limit resonance structures is not always straightforward. According to the commonly adopted guidelines, which we briefly summarize here for the reader's convenience, the most significant resonance structure has:

A. the greatest number of full octets (or if applicable, expanded octets);

B. the least number of atoms with formal charges;

C. negative formal charges on the most electronegative atoms, and positive formal charges on the least electronegative atoms;

D. the greatest number of covalent bonds;

E. π-bond, if present, between atoms of the same row of the periodic table (usually carbon π-bonded to boron, carbon, nitrogen, oxygen, or fluorine).

F. Furthermore, aromatic resonance structures are more significant than non-aromatic ones.

Before analyzing the main resonance structures for the cuprous complexes herein considered, it is worth recalling that cuprous ion (Cu^+) features a $[Ar]3d^{10}$ electronic configuration, i.e. 3d orbitals are completely filled. Therefore, resonance structures featuring additional ligand-to-metal π-donation are not allowed. Moreover, resonance structures involving net electron loss on nitrogen will not be considered, since they would deeply disregard

guideline **C**. It is noteworthy that the resonance structures issuing from the above rules always coincide with the most probable ones predicted by NRT (see Tab. 2), which have a percentage above 90 % except for compounds 5 and 6, where the methyl group is involved in hyperconjugative interactions (vide infra).

3.1 CuCN and CuNC

The most significant resonance structures for each of the two possible complexes of Cu^+ with CN^- are:

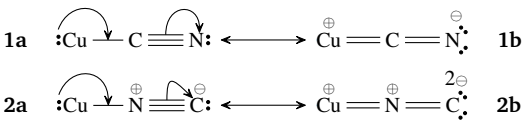

where the Lewis electron pair on Cu denotes 3d electrons available for metal-to-ligand π-backdonation. For both CuCN and CuNC, the left-hand-side structures (**1a** and **2a**) result from simple σ donation from the C and N lone pairs, respectively, of $:\overset{\ominus}{C}\equiv N:$. In both cases, these two structures are more important than the right-hand-side ones, although it should be noted that the CuNC structure **2a** features charge separation, thus justifying the fact that, as known, the CuCN is by far the preferred isomer. In fact, the CuCN resonance structure **1b** features charge separation with respect to **1a**, thus disregarding guideline **B**, though still fulfilling guideline **C**; as for CuNC, resonance structure **2b** features a positive charge on Cu, on the opposite side with respect to the carbon atom which bears a double negative formal charge, thus displaying a greater charge separation and largely disregarding guidelines **B** and **C**.

On the other hand, another resonance structure (**2c**) can be written for CuNC:

resulting from intra-ligand charge rearrangement (polarization) of the electron cloud of C and N. Focusing on the C atom, the limit resonance structure **2c** disregards guideline **A**, but it fulfills guideline **B**, thus probably gaining some importance.

On the basis of this analysis, the metal-ligand bond in CuCN should feature prominent σ-donation and some metal-to-ligand π-back-donation, while that in CuNC should feature σ-donation and mainly electron density rearrangement internal to the ligand moiety.

3.2 $CuCNH^+$ and $CuNCH^+$

Analogous formulae can be written for the second pair of complexes considered in this work (resulting from protonation of CuCN and CuNC), that is $CuCNH^+$ and $CuNCH^+$:

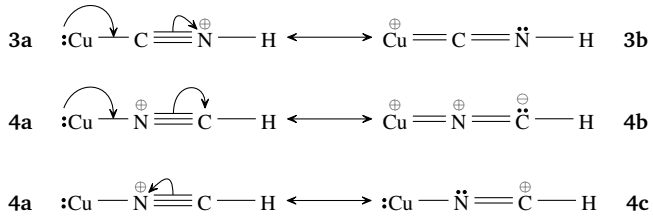

However, in this case the right-hand-side formulae are expected to gain more importance than in the unprotonated complexes due to the presence of H^+, which leads to a less pronounced charge separation.

Accordingly, the protonated species should behave similarly to the respective neutral complexes on a qualitative ground, but π backdonation in $CuCNH^+$ and $CuNCH^+$ should be enhanced with respect to the unprotonated species. Also, intra-ligand polarization in $CuNCH^+$ should result enhanced with respect to the unprotonated species.

3.3 $CuCNCH_3^+$ and $CuNCCH_3^+$

Also for the third and last pair of compounds, $CuCNCH_3^+$ and $CuNCCH_3^+$, the main resonance formulae are analogous to those discussed above:

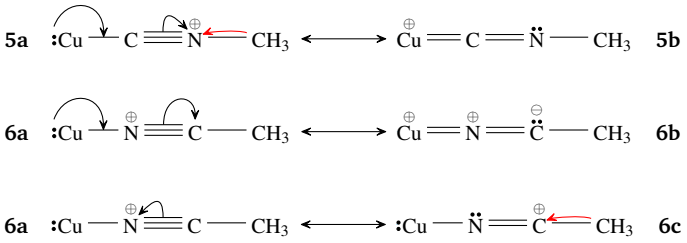

and the relative importance of the left- versus right-hand-side formulae should reflect that in $CuCNH^+$ and $CuNCH^+$, as also here there is a less pronounced charge separation.

However, for these compounds the additional phenomenon of hyperconjugation (depicted in the formulae by means of red arrows) is expected to show up: the electron pairs of the three σ C–H bonds in the methyl group may indeed be delocalized towards the adjacent π^* molecular orbital around the C and N atoms, the same that accepts charge through π backdonation from the metal. As the structure resulting from hyperconjugation is the right-hand-side (the less important) one for $CuCNCH_3^+$ and the left-hand-side (the more important) one for $CuNCCH_3^+$, hyperconjugation can be expected to be greater in this latter complex.

4 Quantitative analysis

A synopsis of the results obtained through our analysis for the six considered systems is given in Tab. 3. For each complex, the first seven NOCV components of $\Delta\rho(x,y,z)$ are grouped into five chemically meaningful charge-flow channels (two of which have π symmetry and result, each, from summation of two degenerate NOCV components). For each channel, the related NOCV-component index/es are given, together with the associated weight factor and charge-transfer (CT) value.

These charge-flow channels are qualitatively similar for all the considered complexes, and their nature will be illustrated in deeper detail (through a visual analysis of the related NOCVs) for the case of CuCN. The analysis will then, for all complexes, focus on quantitative aspects by means of the charge-flow profile associated with each channel.

For purposes of comparison with a different approach, the CT values and the other terms of the NEDA analysis of the six systems are reported in Tab. 4. Since general trends are comparable we will discuss in the following only the results issuing from the NOCV analysis.

As done in Section 3, the results will be presented for the complex pairs CuCN and CuNC (Sec. 4.1), $CuCNH^+$ and $CuNCH^+$ (Sec. 4.2), and $CuCNCH_3^+$ and $CuNCCH_3^+$ (4.3).

4.1 CuCN and CuNC

Figure 1 shows the NOCV pairs, φ_{-k} and φ_k, and the associated charge-rearrangement, $\Delta\rho_k$, for the first seven NOCV components indexed in order of decreasing weight factor for complex CuCN. Recall that, within the NOCV scheme, each partial charge flow $w_k\Delta\rho_k$ results from w_k electrons flowing from orbital φ_{-k} to orbital φ_k.

The first component ($k = 1$) has a clear σ-donation (**σ-don** hereinafter) character from the CN^- HOMO to the metal centre, which in turn also undergoes an internal charge redistribution drawing charge from a d_z orbital and thus flattening, as evidenced in Ref. 24, to some extent the electron density around the metal. The second component ($k = 2$) is still of σ symmetry, but shows charge accumulation on the bond segment rather than on one of the fragments; we shall therefore refer to this charge-flow channel as **σ-cov**. The third and fourth components ($k = 3,4$) are clearly two degenerate π-backdonation (abbreviated as **π-back**) components, with C attracting charge not only from the d orbitals of the metal but also from the N electron cloud upon intra-ligand polarization (see also Ref. 19 on this aspect). The fifth, sixth, and seventh components, of π ($k = 5,6$) and σ ($k = 7$) symmetry, do not show any charge transfer/sharing character, but rather a (modest, as we shall see) intra-fragment polarization of the electron cloud, and shall be therefore labeled as **π-pol** and **σ-pol**, respectively.

As already mentioned, this qualitative picture holds for all the complexes considered in this work, with minor differences in the relative importance (i.e. magnitude of the weight factor) of the NOCV components, which are summarized in Table 3. A closer inspection at these weight factors shows that in all complexes the most important contribution is σ-don, closely followed by π-back, and that these two channels are separated roughly by a factor two from the remaining (less important) channels. As will be discussed shortly, NOCV components with $k > 7$ contribute to a negligible extent to the overall charge redistribution.

Charge-flow profiles for the five highlighted charge-flow channels upon Cu^+-cyanide bonding in CuCN (left) and CuNC (right) are given in Figure 2. The overall charge-flow profile (i.e., that associated with $\Delta\rho$) is shown as a black solid line. The charge-flow profiles associated with the above highlighted five channels are also shown according to the following color scheme: σ-don, red solid line; π-back, blue solid line; σ-cov, light-red dashed line; π-pol, light-blue solid line; σ-pol, light-red solid line. A gray vertical line marks the boundary between the two fragments (as formulated in Section 2). Charge-flow profiles associated with NOCV components with k from 8 to 12 are also shown as gray solid lines; as apparent, these are everywhere almost-flat curves and as already mentioned contribute negligibly to the overall charge redistribution.

On inspection of Fig. 2, one can see that in both CuCN and CuNC the overall charge-flow profile is positive throughout the z axis. This means that the charge-flow is always in the direction from the ligand to the metal (from right to left). As already mentioned, such overall charge flow results from summation of the NOCV components and is almost completely recovered by the first seven of them. Focusing on these components, the most important are certainly the σ-don and π-back ones. The charge-flow profile of σ-don is, as expected, positive almost everywhere in both complexes, and is markedly more pronounced in CuCN than in CuNC, with associated CT 0.261 e versus 0.196 e (see Table 3), respectively. This ligand-to-metal donation is complemented by a CT of -0.035 e for CuCN and -0.017 e for CuNC associated with the σ-cov channel, which shows indeed a partial charge-transfer character due to unbalanced electron sharing from the fragments. On the contrary, in both complexes the π-back charge-flow profile is negative in the region around the Cu nucleus and positive in the region around the C and N nuclei, and as already mentioned represents in both cases metal-to-ligand π backdonation and polarization of the ligand electron cloud in the direction from right to left. The π-back charge-flow profile is higher in CuNC than in CuCN in both the internuclear Cu–C and C–N segments of z, meaning that a weaker π-backdonation and a stronger polarization is occurring in CuNC, perfectly in line with the qualitative analysis of Sec. 3. In fact, the modulus of the negative portion of this charge-flow profile, identifying charge-flow from left to right, i.e. π-backdonation from Cu^+ to cyanide, is more pronounced in CuCN than in CuNC, yielding a CT of -0.016 e (16 me backdonated) against 0.006 e (6 me actually π-donated), which confirms that π-backdonation (as well as structure **1b** of Sec. 3) is barely significant in CuNC. As expected, the remaining channels σ-pol and π-pol have no charge-transfer character (CT of 0.003 e and 0.004 e, respectively).

Indeed, similar conclusions can be achieved with NRT analysis. In both the complexes the **a** is the primary resonance structure and almost the only relevant in CuNC. In agreement with our analysis, the **b** type structure contributes up to 8% in CuCN, whereas it is negligible in CuNC.

4.2 $CuCNH^+$ and $CuNCH^+$

Charge-flow profiles for the main charge-flow channels upon Cu^+-nitrile bonding in $CuCNH^+$ (left) and $CuNCH^+$ (right) are given in Figure 3.

As already mentioned, these complexes are obtained by protonation of CuCN and CuNC, and are therefore a good test case to probe the electrostatic effect induced by addition of a proton. In both these cases, the σ-don charge-flow profile is lowered with respect to the unprotonated species (yielding a CT of 0.182 e for $CuCNH^+$ and 0.117 e for $CuNCH^+$) due to attraction of the electron cloud by the positive proton charge. On the same note, the π-back charge-flow profile is everywhere lowered with respect to the unprotonated species. This also means that, as predicted by the analysis of the resonance structures in Sec. 3, a stronger π backdonation is occurring in $CuCNH^+$ (CT of -0.065 e) and $CuNCH^+$ (-0.032 e) than in CuCN and CuNC, respectively.

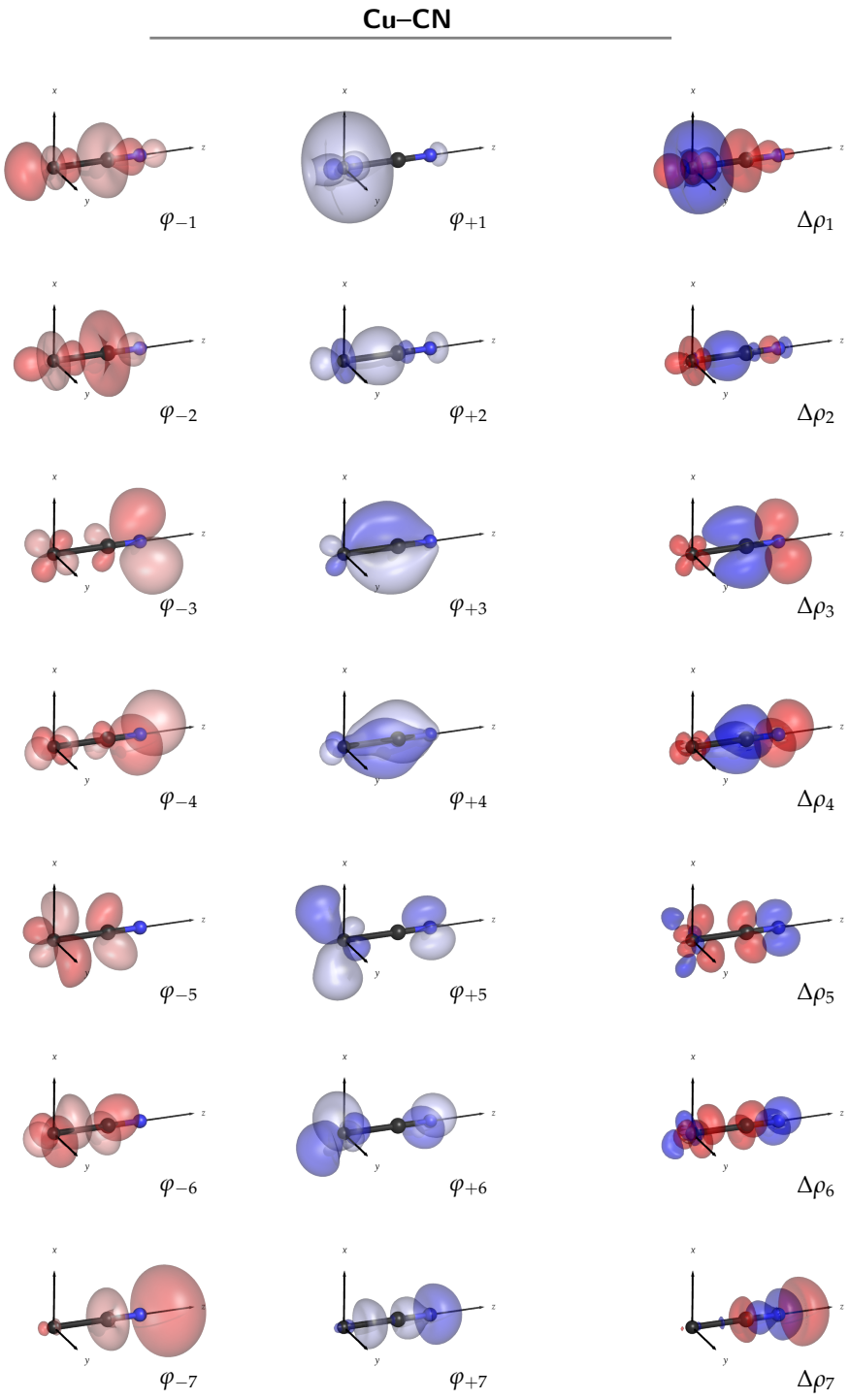

Fig. 1: NOCV pairs (φ_{-k} and φ_k, isodensity surfaces at ± 0.05 (e/bohr^3)$^{1/2}$) and associated charge rearrangement ($\Delta\rho_k$, isodensity surfaces at $\pm$ 0.005 e/bohr^3) for the first seven charge-rearrangement components upon bonding of Cu^+ to CN^- in CuCN. In $\Delta\rho_k$ plots, red isosurfaces represent regions of electron depletion, blue isosurfaces represent regions of electron accumulation.

Table 3: Weights (NOCV eigenvalues w_k) and ligand-to-metal charge transfers (CTs) for the six cuprous complexes considered in this work. Note that the π-back and π-pol channels result each from summation of two degenerate NOCV components, and so does the related weight and charge transfer.

	CuCN			CuNC			$CuCNH^+$			$CuNCH^+$			$CuCNCH_3^+$			$CuNCCH_3^+$		
channel	k	w_k	CT	k	w_k	CT	k	w_k	CT	k	w_k	CT	k	w_k	CT	k	w_k	CT
σ-don	1	0.55	0.261	1	0.57	0.196	1	0.44	0.182	1	0.40	0.117	1	0.46	0.190	1	0.42	0.126
π-back	3,4	0.37	-0.016	2,3	0.38	0.006	2,3	0.42	-0.065	2,3	0.37	-0.032	2,3	0.43	-0.055	2,3	0.39	-0.023
σ-cov	2	0.23	-0.035	4	0.19	-0.017	4	0.18	-0.020	4	0.13	-0.002	4	0.18	-0.019	4	0.13	-0.001
π-pol	5,6	0.20	0.003	6,7	0.21	0.006	5,6	0.12	0.004	5,6	0.12	0.007	5,6	0.13	0.004	5,6	0.13	0.008
σ-pol	7	0.09	0.004	5	0.12	0.014	7	0.05	0.000	7	0.06	0.001	7	0.06	0.000	7	0.06	0.001

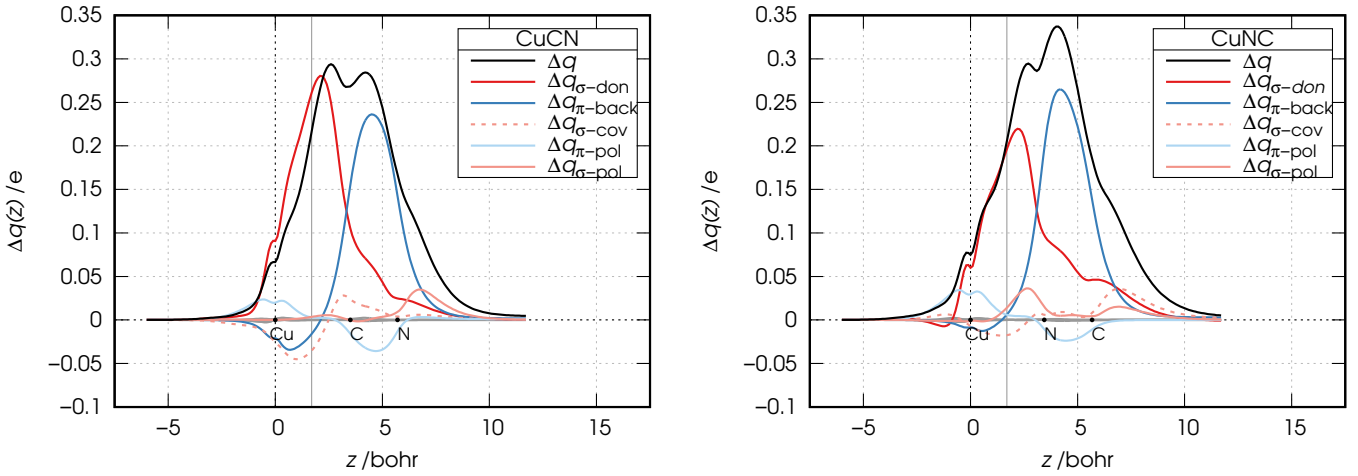

Fig. 2: Charge-flow profiles of the main charge-flow channels upon bonding in Cu–CN and Cu–NC (charge-flow profiles for channels corresponding to NOCVs with k ranging from 8 to 12 are also shown in gray color, while the overall charge-flow profile is given as a black line).

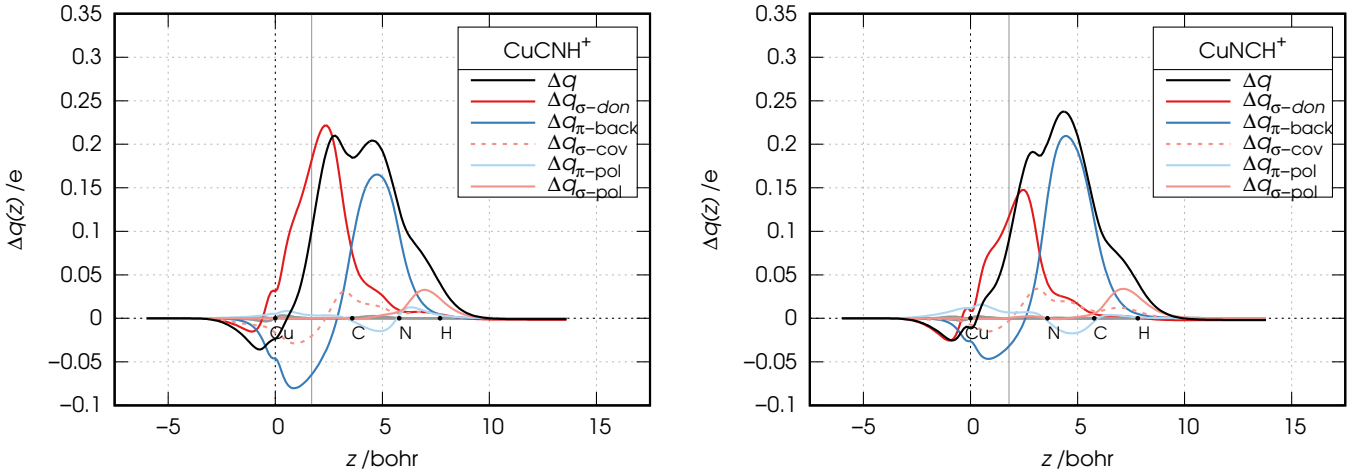

Fig. 3: Charge-flow profiles of the main five charge-flow channels upon bonding in Cu–CNH^+ and Cu–NCH^+ (charge-flow profiles for channels corresponding to NOCVs with k ranging from 8 to 12 are also shown in gray color, while the overall charge-flow profile is given as a black line).

Table 4: Natural energy decomposition analysis (NEDA) components in kcal mol^{-1}. The Core, electronic and charge transfer (CT) contributions are reported.

Species	Core	Elec.	CT	Tot.
CuCN	195.1	-286.5	-93.5	-184.9
CuNC	158.9	-272.2	-59.7	-173.0
$CuCNH^+$	141.8	-141.7	-59.6	-59.5
$CuNCH^+$	103.4	-119.4	-33.0	-49.0
$CuCNCH_3^+$	149.3	-154.9	-62.8	-68.4
$CuNCCH_3^+$	111.2	-133.5	-36.3	-58.7

4.3 $CuCNCH_3^+$ and $CuNCCH_3^+$

Charge-flow profiles for the five highlighted charge-flow channels upon Cu^+-nitrile bonding in $CuCNCH_3^+$ (left) and $CuNCCH_3^+$ (right) are given in Figure 4.

These complexes are obtained by addition of CH_3^+ to CuCN and CuNC and, as mentioned in Sec. 3, should feature a similar electrostatic effect as in the protonated complexes discussed in Sec. 4.2. For both $CuCNCH_3^+$ and $CuNCCH_3^+$, the charge-flow profiles of all five channels are indeed very similar to those of $CuCNH^+$ and $CuNCH^+$, respectively (with a CT of 0.190 e for σ-don and -0.055 e for π-back in $CuCNCH_3^+$, and a CT of 0.126 e for σ-don and -0.023 e for π-back in $CuNCCH_3^+$).

However, as anticipated by the analysis of the resonance structures in Sec. 3, a peculiar feature of these two complexes should be the hyperconjugation phenomenon involving delocalization of the electron pairs of the three C–H bond of the methyl group in a π^* molecular orbital on the C–N atoms. Further insight on this aspect can be gained by a detailed inspection of the NOCV components where this molecular orbital is mostly involved (as highlighted in Tab. 3, those – degenerate – with $k = 2$ and 3). The NOCV pairs for $k = 2$ and 3 are to this purpose reported in Fig. 5 and indeed show, in a strikingly clear way, the hyperconjugation phenomenon. In particular, the two pairs clearly show the formation of two degenerate π bonding lobes with participation from the three C–H σ bonds of the methyl group and the lobes of a π^* molecular orbital on the C and N atoms. This reflects in the related charge-flow profiles in Fig. 4 showing a positive peak (charge flow from right to left) in the CH_3 region. Also, in line with the predictions made in Sec. 3 through the analysis of the resonance structures, a stronger hyperconjugation (a higher peak) is recorded for $CuNCCH_3^+$. The crucial role played by methyl group is also confirmed by the NRT analysis. As reported in Tab. 2, the weight of the primary structure decreases in favor of secondary resonance structures. If we consider the most relevant secondary structures of $CuCNCH_3^+$, the σ CH bond is equally delocalized between the π^* and the hydrogen, on the other hand, in the $CuNCCH_3^+$ complex the first three secondary structure (covering more the 10% of the resonance structures weight) resent of the hyperconjugation effect.

5 Conclusions

In this work, we investigated chemical bonding from the perspective of electron charge redistribution in cuprous complexes with simple nitriles by comparing qualitative models based on the simple popular octet rule and resonance concepts with the results of a recently developed quantitative analysis scheme based on quantum-mechanical calculations and framed within density-functional theory. The set of studied complexes (CuCN, CuNC, $CuCNH^+$, $CuNCH^+$, $CuCNCH_3^+$, and $CuNCCH_3^+$) was designed by adding complexity to the simple copper(I) cyanide, an important reagent in organic, organometallic, and supramolecular chemistry, through a series of ligands that are themselves of interest in diverse fields including coordination chemistry, astrochemistry, and catalysis.

In agreement with a preliminary analysis of the resonance structures for the six considered complexes, our results show that i) the main charge-flow channel in the metal-ligand bonding is σ donation followed by π backdonation; ii) π backdonation has a larger weight when Cu is bound to C rather than to N; iii) the polarization of the electron cloud around C and N in the direction pointing to the metal is greater when Cu is bound to N rather than to C; iv) the addition of a positively charged fragment (H^+ or CH_3^+) significantly enhances π backdonation; v) hyperconjugation in the last two complexes can be effectively singled out and quantified, and is found to be larger in $CuNCCH_3^+$ than in $CuCNCH_3^+$.

Besides their specific interest for a better understanding of chemical bonding in the considered cuprous complexes, our results show that such a central concept as the rearrangement of electrons upon formation of a chemical bond can nowadays be modeled and computed within a quantum mechanical framework and successfully analyzed for a one to one comparison with widely employed models such as the octet rule and the resonance structures, and for a deeper insight into the studied chemical bonds.

Acknowledgements

The research leading to these results has received funding from Scuola Normale Superiore through project “DIVE: Development of Immersive approaches for the analysis of chemical bonding through Virtual-reality Environments” (SNS18_B_RAMPINO) and program “Finanziamento a supporto della ricerca di base” (SNS_RB_RAMPINO). The results were obtained through a parallel computer code partly developed within the Project HPC-EUROPA3 (INFRAIA-2016-1-730897), with the support of the EC Research Innovation Action under the H2020 Programme; in particular, S.R. gratefully acknowledges the support of Prof. Carole Morrison of the School of Chemistry of the University of Edinburgh, and the computer resources and technical support provided by the Edinburgh Parallel Computing Centre.

Conflicts of interest

There are no conflicts to declare.

Notes and references

1 G. N. Lewis, *J. Am. Chem. Soc.*, 1916, **38**, 762–785.
2 R. J. Gillespie and E. A. Robinson, *J. Comput. Chem.*, 2007, **28**, 87–97.
3 R. Abegg, *Z. Anorg. Chem.*, 1904, **39**, 330–380.
4 I. Langmuir, *J. Am. Chem. Soc.*, 1919, **41**, 868–934.
5 N. V. Sidgwick and H. M. Powell, *Proc. R. Soc. London, Ser. A*, 1940, **176**, 153–180.
6 R. J. Gillespie, *J. Chem. Educ.*, 1970, **47**, 18–23.
7 W. Heisenberg, *Z. Phys.*, 1926, **39**, 499–518.
8 L. Pauling, *Chem. Rev.*, 1928, **5**, 173–213.

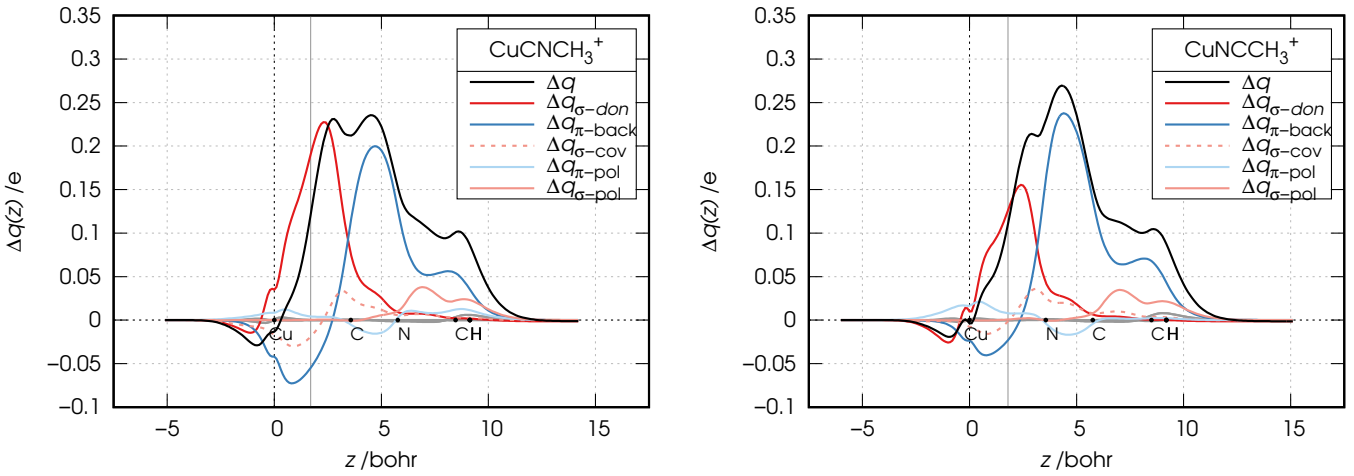

Fig. 4: Charge-flow profiles of the main charge-flow channels upon bonding in Cu–$CNCH_3^+$ and Cu–$NCCH_3^+$ (charge-flow profiles for channels corresponding to NOCVs with k ranging from 8 to 12 are also shown in gray color, while the overall charge-flow profile is given as a black line).

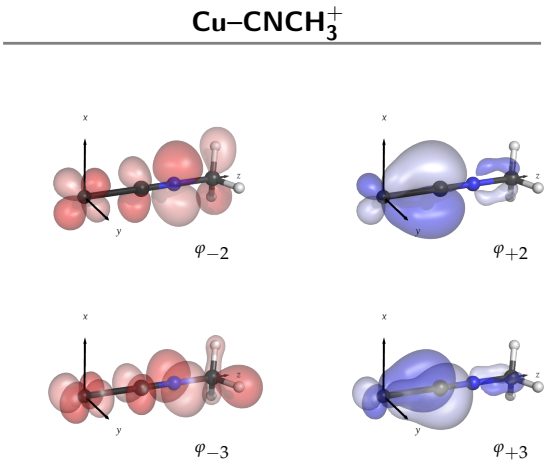

Fig. 5: NOCV pairs (φ_{-k} and φ_k, isodensity surfaces at ± 0.05 $(e/bohr^3)^{1/2}$) for charge-rearrangement components $k = 2$ and 3 relating to π backdonation and hyperconjugation in Cu–$CNCH_3^+$.

9 L. Pauling, *J. Am. Chem. Soc.*, 1931, **53**, 3225–3237.
10 L. Pauling and J. Sherman, *J. Chem. Phys.*, 1933, **1**, 679–686.
11 I. Langmuir, *Science*, 1921, **54**, 59–67.
12 *The Chemical Bond*, ed. G. Frenking and S. Shaik, Wiley-VCH Verlag GmbH & Co. KGaA, Weinheim, 2014.
13 J. Bogumil, R. Moszynski and K. Szalewicz, *Chem. Rev.*, 1994, **94**, 1887–1930.
14 K. Szalewicz, *WIRES Comput. Mol. Sci.*, 2012, **2**, 254–272.
15 L. Zhao, M. von Hopffgarten, D. M. Andrada and G. Frenking, *WIRES Comput. Mol. Sci.*, 2018, **8**, e–1345.
16 R. Bader, *Chem. Rev.*, 1991, **91**, 893–928.
17 A. Savin, O. Jepsen, J. Flad, H. Preuss and H. G. Schnering, *Angew. Chem. Int. Ed. Engl.*, 1992, **31**, 187–188.
18 O. Savin, A.a nd Jepsen, J. Flad, H. Preuss and H. G. Schnering, *J. Comput. Chem.*, 2010, **31**, 1504–1519.
19 A. Salvadori, M. Fusè, G. Mancini, S. Rampino and V. Barone, *J. Comput. Chem.*, 2018, **39**, 2607–2617.
20 J. Lupi, M. Martino, A. Salvadori, S. Rampino, G. Mancini and V. Barone, *AIP Conf. Proc.*, 2019, **2145**, 020001.
21 G. Bistoni, S. Rampino, N. Scafuri, G. Ciancaleoni, D. Zuccaccia, L. Belpassi and F. Tarantelli, *Chem. Sci.*, 2016, **7**, 1174–1184.
22 M. Fusè, I. Rimoldi, E. Cesarotti, S. Rampino and V. Barone, *Phys. Chem. Chem. Phys.*, 2017, **19**, 9028–9038.
23 M. Fusè, I. Rimoldi, G. Facchetti, S. Rampino and V. Barone, *Chem. Commun.*, 2018, **54**, 2397–2400.
24 M. De Santis, S. Rampino, L. Storchi, L. Belpassi and F. Tarantelli, *Inorg. Chem.*, 2019, **58**, 11716–11729.
25 W. Li, L. Spada, N. Tasinato, S. Rampino, L. Evangelisti, A. Gualandi, P. G. Cozzi, S. Melandri, V. Barone and C. Puzzarini, *Angew. Chem., Int. Ed.*, 2018, **57**, 13853–13857.
26 D. A. Obenchain, L. Spada, S. Alessandrini, S. Rampino, S. Herbers, N. Tasinato, M. Mendolicchio, P. Kraus, J. Gauss, C. Puzzarini, J.-U. Grabow and V. Barone, *Angew. Chem., Int. Ed.*, 2018, **57**, 15822–15826.
27 A. Patti, S. Pedotti, G. Mazzeo, G. Longhi, S. Abbate, L. Paoloni, J. Bloino, S. Rampino and V. Barone, *Phys. Chem. Chem. Phys.*, 2019, **21**, 9419–9432.
28 D. B. Grotjahn, M. A. Brewster and L. M. Ziurys, *J. Am. Chem. Soc.*, 2002, **124**, 5895–5901.
29 R. O. Ramabhadran, Y. Hua, A. H. Flood and K. Raghavachari, *J. Phys. Chem. A*, 2014, **118**, 7418–7423.
30 A. G. Sharpe, *The chemistry of cyano complexes of the transition metals*, Academic Press London ; New York, 1976.
31 M. A. Cordiner, A. J. Remijan, J. Boissier, S. N. Milam, M. J. Mumma, Charnley, L. Paganini, G. Villanueva, D. Bockelée-Morvan, Y.-J. Kuan, Y.-L. Chuang, D. C. Lis, N. Biver, J. Crovisier, D. Minniti and I. M. Coulson, *Astrophys. J. Letters*, 2014, **792**, L2.
32 S. B. Charnley, S. D. Rodgers, H. M. Butner and P. Ehrenfreund, *Earth, Moon, and Planets*, 2002, **90**, 349–360.
33 E. Rissi, R. Rivelino and S. Canuto, *Int. J. Quantum. Chem.*, **91**, 575–585.
34 B. S. Jursic, *J. Chem. Soc., Faraday Trans.*, 1997, **93**, 2355–2359.
35 F. Pichierri, *Chem. Phys. Lett.*, 2002, **353**, 383–388.
36 E. Sarrasin, D. B. Abdallah, M. Wernli, A. Faure, J. Cernicharo and F. Lique, *Mon. Not. R. Astron. Soc.*, 2010, **404**, 518–526.
37 C. Eric Cotton, J. S. Francisco and W. Klemperer, *J. Chem. Phys.*, 2013, **139**, 014304.
38 S. A. Di Biase, J. R. Beadle and G. W. Gojel, *Organic Syntheses*, 1984, **62**, 179.
39 S. F. Rach and F. E. Kühn, *Chem. Rev.*, 2009, **109**, 2061–2080.
40 I. V. Alabugin, K. M. Gilmore and P. W. Peterson, *Wiley Interdiscip. Rev.: Comput. Mol. Sci.*, **1**, 109–141.
41 G. Bistoni, S. Rampino, F. Tarantelli and L. Belpassi, *J. Chem. Phys.*, 2015, **142**, 084112.
42 M. De Santis, S. Rampino, H. M. Quiney, L. Belpassi and L. Storchi, *J. Chem. Theory. Comput.*, 2018, **14**, 1286–1296.
43 L. Storchi, S. Rampino, L. Belpassi, F. Tarantelli and H. M. Quiney, *J. Chem. Theory. Comput.*, 2013, **9**, 5356–5364.
44 S. Rampino, L. Belpassi, F. Tarantelli and L. Storchi, *J. Chem. Theory. Comput.*, 2014, **10**, 3766–3776.
45 M. Mitoraj and A. Michalak, *J. Mol. Model.*, 2007, **13**, 347–355.
46 M. Radoń, *Theor. Chem. Acc.*, 2008, **120**, 337–339.
47 L. Belpassi, I. Infante, F. Tarantelli and L. Visscher, *J. Am. Chem. Soc.*, 2008, **130**, 1048–1060.
48 S. Rampino, L. Storchi and L. Belpassi, *J. Chem. Phys.*, 2015, **143**, 024307 (8).
49 M. J. Frisch, G. W. Trucks, H. B. Schlegel, G. E. Scuseria, M. A. Robb, J. R. Cheeseman, G. Scalmani, V. Barone, G. A. Petersson, H. Nakatsuji, X. Li, M. Caricato, A. V. Marenich, J. Bloino, B. G. Janesko, R. Gomperts, B. Mennucci, H. P. Hratchian, J. V. Ortiz, A. F. Izmaylov, J. L. Sonnenberg, D. Williams-Young, F. Ding, F. Lipparini, F. Egidi, J. Goings, B. Peng, A. Petrone, T. Henderson, D. Ranasinghe, V. G. Zakrzewski, J. Gao, N. Rega, G. Zheng, W. Liang, M. Hada, M. Ehara, K. Toyota, R. Fukuda, J. Hasegawa, M. Ishida, T. Nakajima, Y. Honda, O. Kitao, H. Nakai, T. Vreven, K. Throssell, J. A. Montgomery, Jr., J. E. Peralta, F. Ogliaro, M. J. Bearpark, J. J. Heyd, E. N. Brothers, K. N. Kudin, V. N. Staroverov, T. A. Keith, R. Kobayashi, J. Normand, K. Raghavachari, A. P. Ren-

dell, J. C. Burant, S. S. Iyengar, J. Tomasi, M. Cossi, J. M. Millam, M. Klene, C. Adamo, R. Cammi, J. W. Ochterski, R. L. Martin, K. Morokuma, O. Farkas, J. B. Foresman and D. J. Fox, *Gaussian 16 Revision C.01*, 2016, Gaussian Inc. Wallingford CT.
50 C. Lee, W. Yang and R. G. Parr, *Phys. Rev. B*, 1988, **37**, 785–789.
51 A. D. Becke, *J. Chem. Phys.*, 1993, **98**, 5648–5652.
52 S. Grimme, S. Ehrlich and L. Goerigk, *J. Comput. Chem.*, 2011, **32**, 1456–1465.
53 P. J. Hay and W. R. Wadt, *J. Chem. Phys.*, 1985, **82**, 270–283.
54 P. C. Hariharan and J. A. Pople, *Theor. Chim. Acta*, 1973, **28**, 213–222.
55 T. Clark, J. Chandrasekhar, G. W. Spitznagel and P. V. R. Schleyer, *J. Comput. Chem.*, 1983, **4**, 294–301.
56 L. Goerigk and S. Grimme, *WIREs Comput Mol Sci*, 2014, **4**, 576–600.
57 C. Puzzarini, J. Bloino, N. Tasinato and V. Barone, *Chem. Rev.*, 2019, **119**, 8131–8191.
58 S. Alessandrini, V. Barone and C. Puzzarini, *J. Chem. Theory Comput.*, 2020, **16**, 988–1006.
59 G. Santra, N. Sylvetsky and J. M. Martin, *J. Phys. Chem. A*, 2019, **123**, 5129–5143.
60 E. Papajak, J. Zheng, X. Xu, H. R. Leverentz and D. G. Truhlar, *J. Chem. Theory Comput.*, 2011, **7**, 3027–3034.
61 K. A. Peterson and C. Puzzarini, *Theor. Chem. Acc.*, 2005, **114**, 283–296.
62 D. Figgen, G. Rauhut, M. Dolg and H. Stoll, *J. Chem. Phys.*, 2005, **311**, 227–244.
63 E. Glendening and F. Weinhold, *J. Comput. Chem.*, 1998, **19**, 593–609.
64 E. D. Glendening and A. Streitwieser, *J. Chem. Phys.*, 1994, **100**, 2900–2909.
65 E. D. Glendening, *J. Am. Chem. Soc.*, 1996, **118**, 2473–2482.
66 E. D. Glendening, *J. Phys. Chem. A*, 2005, **109**, 11936–11940.
67 E. D. Glendening, J. K. Badenhoop, A. E. Reed, J. E. Carpenter, J. A. Bohmann, C. M. Morales, P. Karafiloglou, C. Landis and F. Weinhold, *NBO 7.0*, 2018, Theoretical Chemistry Institute, University of Wisconsin, Madison.
68 J. Grant Hill, A. O. Mitrushchenkov and K. A. Peterson, *J. Chem. Phys.*, 2013, **138**, 134314.
69 F. M. Bickelhaupt and K. N. Houk, *Angew. Chem. Int. Ed.*, 2017, **56**, 10070–10086.
70 O. Dietz, V. M. Rayón and G. Frenking, *Inorg. Chem.*, 2003, **42**, 4977–4984.
71 S. Rampino, *The Waverley program package*, http://www.srampino.com/code.html#Waverley, Accessed February 20, 2018.
72 S. Rampino, *VIRT&L-COMM*, 2015, **7**, 6.